Article

How suitable is MALDI-TOF for metabolite imaging from clinical formalin-fixed and paraffin-embedded tissue samples in comparison to MALDI-FT-ICR mass spectrometry?

Achim Buck, Benjamin Balluff, Andreas Voss, Rupert Langer, Horst Zitzelsberger, Michaela Aichler, and Axel Walch

Anal. Chem., **Just Accepted Manuscript** • DOI: 10.1021/acs.analchem.6b00460 • Publication Date (Web): 11 Apr 2016

How suitable is MALDI-TOF for metabolite imaging from clinical formalin-fixed and paraffin-embedded tissue samples in comparison to MALDI-FT-ICR mass spectrometry?

Achim Buck[1], Benjamin Balluff[2], Andreas Voss[1], Rupert Langer[3], Horst Zitzelsberger[4], Michaela Aichler[1], and Axel Walch[1]*

[1]Research Unit Analytical Pathology, Helmholtz Zentrum München, Neuherberg, Germany
[2]Maastricht MultiModal Molecular Imaging Institute (M4I), Maastricht University, Maastricht, The Netherlands
[3]Institute of Pathology, University of Bern, Bern, Switzerland
[4]Research Unit Radiation Cytogenetics, Helmholtz Zentrum München, Neuherberg, Germany

*Corresponding author: A Walch, MD, Research Unit Analytical Pathology, Helmholtz Zentrum München, Ingolstädter Landstrasse 1, 85764 Neuherberg, Germany.
E-mail: axel.walch@helmholtz-muenchen.de

The authors declare no competing financial interests.

ABSTRACT

In research and clinical settings formalin-fixed and paraffin-embedded (FFPE) tissue specimens are collected routinely and therefore this material constitutes a highly valuable source to gather insight in metabolic changes of diseases. Among mass spectrometry techniques to examine the molecular content of FFPE tissue mass spectrometry imaging (MSI) is the most appropriate when morphological and histological features shall be related to metabolic information. Currently, high resolution mass spectrometers are widely used for metabolomics studies. However, with regards to matrix-assisted laser desorption/ionization (MALDI) MSI no study has so far addressed the necessity of instrumental mass resolving power in terms of clinical diagnosis and prognosis using archived FFPE tissue. For this matter we performed for the first time a comprehensive comparison between a high mass resolution Fourier-transform ion cyclotron resonance (FT-ICR) mass spectrometer and a time-of-flight (TOF) instrument with lower mass resolving power. Spectra analysis revealed that about one third of the detected peaks remained unresolved by MALDI-TOF which led to a three to five time lower number of *m/z* features compared to FT-ICR measurements. Overlaid peak information and background noise in TOF images made a precise assignment of molecular attributes to morphological features more difficult and limited classification approaches. This clearly demonstrates the need for high mass resolution capabilities for metabolite imaging. Nevertheless, MALDI-TOF allowed reproducing and verifying individual markers identified previously by MALDI-FT-ICR MSI. The systematic comparison gives rise to synergistically combine the different MSI platforms for high-throughput discovery and validation of biomarkers.

INTRODUCTION

The capability of mass spectrometry imaging (MSI) to cover highly sensitive and specific numerous molecular classes (e.g. proteins, peptides, glycans, and metabolites) together with information of the *in situ* distribution profiles has given rise to examine tissue molecular signatures in terms of histology-based diagnostic and research purposes.[1-5] Mass spectrometry studies, based on liquid- and gas-chromatography MS, have shown that metabolites are retained in formalin-fixed, paraffin-embedded (FFPE) tissue samples.[6-9] Using a matrix-assisted laser desorption/ionization Fourier-transform ion cyclotron resonance (MALDI-FT-ICR) MSI platform, we have recently demonstrated that metabolites are not only chemical, but also spatial preserved in FFPE tissue specimens which allows the comprehensive analysis of metabolites in a histological context.[10] This approach permits high-throughput *in situ* metabolomics for diagnostic and research purposes opening the vast number of archived FFPE tissue collections for MSI analysis.

With regards to MALDI MSI there are at present two main categories of mass spectrometers used for small molecule imaging: time-of-flight (TOF) and fourier transform MS, including Orbitrap and FT-ICR MS. TOF mass analyzers are currently the most widely used analyzers for imaging experiments, mostly due to their good analytical sensitivity, relative low cost compared to other systems and high duty cycle. In contrast, Orbitrap and FT-ICR MS are high performance mass analyzers which are achieving highest levels of resolving power ($m/\Delta m$) with 100,000 or even more. As mass resolution of FT-ICR MS instruments improve by increase in magnetic field strength.[11,12] Furthermore, mass resolving power is directly proportional to the length of the time-domain signal.[13] However, the practicality of an imaging experiment is limited by the length of acquisition time due to extended measurement times when analyzing cohorts of large tissue sections. Additionally, high mass resolution MS delivers a large amount of mass spectral data with one spectrum file containing millions of data points. Large numbers of spectra present a challenge in data handling and analyzing. Thus, long acquisition times together with high data information obtained from high performance analyzers can lower experimental throughput and investigators have to balance between acquisition speed and used spatial resolution (typically in the range of 10 to 100 µm) which determines step size of tissue raster pattern. In comparison to FT-ICR MS the resolving power of TOF-based instruments is mostly independent of the acquisition rate making them an ideal detector for high-throughput analyzes.[14,15] In recent years, improvements in laser repetition rates (5-10 kHz) combined with continuous raster imaging or continuous stage motion have driven the development of high-speed MALDI-TOF mass spectrometers.[16-18] The capability to quickly analyze large patient tissue cohorts with high

lateral resolution for detailed histology-based molecular information makes TOF instruments nowadays an attractive platform in preclinical and clinical research. Nevertheless, lower mass resolving power remains challenging in metabolite analyses using TOF instruments. We have previously reported that the presence of endogenous and matrix causing signals can mask analytes of interest in the low-mass range by using a MALDI-TOF device. [19,20] In these studies we were interested in the targeted detection of drugs and their corresponding metabolites. Recently, a high-resolution and a medium-resolution mass spectrometer have been used to study neurotransmitters and metabolites from the central nervous system of rodent and crustacean.[21] High resolution mass spectrometry was advantageous to identify analytes of interest directly from tissues via database search.[21] Another bottleneck in MSI concerns the identification of unknown metabolites in imaging studies. High spectral accuracy of isotopic distribution patterns creates the prerequisite to determine elemental composition which can lead to possible metabolite candidate structures.[22-24]

To our knowledge no study has addressed the question of the suitability of MALDI-TOF MSI for global metabolite analysis concerning preclinical and clinical research questions. In clinical practice FFPE tissue specimens are the gold standard for histological and histopathological examination and allow the comparative examination of multiple patient samples when using tissue microarrays (TMAs) for retrospective studies. Recently, we showed that metabolite profiles from FFPE tissue sections can be used to discriminate between normal and tumor tissues.[10] In this study, data were generated using a FT-ICR MS. Furthermore, the analysis of a TMA containing esophageal adenocarcinomas patient samples resulted in an independent molecular marker which can subdivide patients into different prognostic groups. Following this concept, we measured consecutive tissue sections from the two previous analyzed FFPE TMAs on a MALDI-TOF/TOF mass spectrometer to direct a systematical data comparison of both technologies.

MATERIAL AND METHODS

Tissue preparation

TMAs constructed with tissue samples of colon adenocarcinomas patients (n=28) and esophageal adenocarcinomas (n=53) were used for MALDI MSI analysis as described previously.[10] The resection specimens were processed in a highly standardized manner, opened immediately after surgery and formalin fixation started within the first thirty minutes after resection. The very same procedure of tissue preparation, such as tissue sectioning, deparaffinization, and matrix coating was performed for measurements with MALDI-FT-ICR and MALDI-TOF MSI. FFPE tissue samples were sectioned with a thickness of 4 µm and

mounted onto indium-tin-oxide (ITO)-coated glass slides (Bruker Daltonik GmbH, Bremen, Germany) pretreated with 1:1 poly-L-lysine (Sigma Aldrich, Munich, Germany) and 0.1% Nonidet P-40 (Sigma). FPPE sections were incubated for 1 h at 70°C, deparaffinized in xylene (2 × 8min) and air-dried. For MALDI MSI sections were coated with a solution of 10 mg/ml 9-aminoacridine (Sigma) in 70% methanol using a SunCollect sprayer (Sunchrom, Friedrichsdorf, Germany). Matrix solution was sprayed in eight layers onto the tissue section with the flow rates at 10, 20, 30, and 40 µl/min.

MALDI mass spectrometry imaging

Both MALDI MSI measurements were performed with a step-size of 60 µm lateral resolution in negative ion mode. MALDI FT-ICR MSI (solariX 7 Tesla FT-ICR MS, Bruker) was performed in the mass range of *m/z* 50-1000 with an estimated resolution of 35,000 at *m/z* 400 and an average resolution of ~65,000 over the analyzed mass range (*m/z* 100-1000). Spectra were recorded on solariXcontrol software with 1M data points, a transient length of 0.26 s, and an ion cooling time of 0.01 s. Source conditions were as follows: deflector plate at -200 V, funnel 1 at -150 V, skimmer 1 at -15 V, and with a funnel rf amplitude of 150 Vpp. For each measurement position 100 laser shots were accumulated using a Smartbeam-II Nd:YAG (355 nm) laser operating at a frequency of 500 Hz. External calibration was achieved using L-arginine in the ESI mode. MALDI-time-of-flight measurements were carried out in the reflector mode (*m/z* 80-1000) on an Ultraflex III MALDI-TOF/TOF MS (Bruker) equipped with a Smartbeam-II Nd:YAG laser at a frequency of 100 Hz. The setting for the sampling rate was 2.0 GS/s and a total of 200 laser shots were used for a measurement position. External calibration was performed using peaks from a matrix mix (2,5-dihydroxy-benzoic acid, α-cyano-4-hydroxycinnamic acid and 3,5-Dimethoxy-4-hydroxycinnamic acid). Non-tissue measurements regions were included as background controls to identify matrix peaks. After completion of the measurement the matrix was removed with 70% ethanol, stained with haematoxylin and eosin (H&E) and coverslipped. Digital images were acquired with a 20x magnification objective using a Mirax Desk scanner (Zeiss, Göttingen, Germany). Digitized images were co-registered to respective MSI data using FlexImaging 4.0 (Bruker) and SCiLS Lab version 2015a (SCiLS, Bremen, Germany).

Data processing

Statistical analyses were performed using the software SCiLS Lab version 2015a. Data were loaded and preprocessed according the instrument type for time-of-flight (TOF) and Fourier transform ion cyclotron resonance (FT-ICR). TOF and FT-ICR data were imported separately, axis range was cropped to the mass range *m/z* 100-1000. TOF data were

additionally baseline reduced using a convolution algorithm with the setting of 20 for peak width and normalized to the total ion count (TIC). FT-ICR data were normalized to root mean square (RMS). Histology-guided regions of interests (ROIs) were annotated (e.g. tumor and normal tissue) to generate average mean spectra. Tissue samples of the colon TMA were not annotated and considered in analysis if the sample contained no tumor or normal epithelium, respectively, or if the section was lost during H&E staining. Peak picking was performed on each dataset followed by receiver operating characteristic (ROC) for assessing the discriminatory capacity of groups to be compared. Peak lists were analyzed using Wilcoxon-Rank-Sum test considering the mean spectra of each defined region of interest in the calculation to identify significant differences in *m/z* values. Furthermore, principle component analysis (PCA) was applied on individual spectra groups of datasets.

Global spectra were compared using mMass software version 5.5.0[25] with preprocessed and exported FT-ICR and TOF spectra from SCiLS. Peak picking was done on the average mean spectra of the defined ROIs with s/n ratios of 2.5, 5, 10 and 20 and a picking height of 100. Additionally, shoulder peaks were removed during peak picking of FT-ICR spectra. Spectra were recalibrated to 9-AA because of inherent mass shifts in MALDI-TOF measurements. The *m/z* lists with corresponding intensities, Full Width at Half Maximum (FWHM) and resolution values were exported (.txt file format) and used for further analysis.

The clinicopathologic characteristics of esophageal adenocarcinomas (n = 53) were included in MALDI-TOF and MALDI-FT-ICR analysis. Significance analysis of microarrays (SAM) was used to identify disease-free survival-associated *m/z* values (q-value < 0.05) as described previously ('samr' package in R).[10] Uni- and multivariate statistical survival analyzes were calculated within R ('survival' package).

RESULTS AND DISCUSSION

Two different types of mass spectrometer, a MALDI-FT-ICR and a MALDI-TOF/TOF mass spectrometer were compared comprehensively in terms of the number of detected features, capacity to discriminate between normal and tumor tissue and the discovery of prognostic markers. Recently, we found that metabolite information is spatially and chemically conserved in FFPE tissue specimens which can be used to investigate disease states.[10] In order to ensure comparability the same FFPE patient tissue samples were analyzed on both instrument types. MALDI-TOF showed a nearly linear dependence of the resolving power on *m/z* in the low mass range, whereas mass resolution is inversely proportional in MALDI-FT-ICR MS with higher mass resolution for lower *m/z* species (Figure S-1).[11] On average a mass

resolution of roughly 65,000 was achieved by FT-ICR compared to ~4000 by TOF regarding the detected peaks in the *m/z* range 100-1000 within one measurement.

Mass spectral data comparison

Mass spectra obtained from each instrument type were compared with the same software with parameters comparable and suitable for both mass spectrometers. The same signal-to-noise (s/n) ratios (s/n>2.5, 5, 10, 20) were chosen for each comparison between the mass analyzers. Three to five times more peaks were found in FT-ICR average mean spectrum than in the TOF spectrum (Figure 1A). Peak picking with a s/n>5 yielded peak lists with 1580 features from FT-ICR and 455 features from TOF spectra. The number of obtained features was unequally distributed over the measured *m/z* range (Figure S-2). More *m/z* features were listed in the intervals up to 600 in FT-ICR data whereas the intervals between *m/z* 600-1000 contained similar numbers of features in both data sets. Typically, lipid ions are detected mainly in the mass range above *m/z* 600 which are removed from FFPE tissue samples by solvents during tissue embedding process and paraffin removal.[10,26] This leads to a low number of *m/z* features found in the *m/z* range 600-1000. Nevertheless, it is shown that some solvent resistant lipids are retained and can still be detected from FFPE tissue samples.[10,26] A larger number of detected peaks over the complete measurement range by FT-ICR MS is in accordance with differences in sensitivity and mass resolution of the two mass spectrometers. The higher resolving power of FT-ICR MS becomes important in dealing with the complex molecular nature of tissue samples by better resolving near isobaric species. For a more detailed analysis, peak lists were compared with regard to the number of detected FT-ICR peaks which could be found within the Full Width at Half Maximum (FWHM; peak width measured full at 50% peak height) window of the corresponding TOF peaks (Figure 1B). For examples peaks were considered as common if a single FT-ICR peak was found within the FWHM window of a TOF peak. According to this, 151 TOF peaks were found to have a single related FT-ICR peak whereas 155 TOF peaks have an assignment of two or more detected FT-ICR *m/z* features. Interestingly, 149 features in TOF spectra and 1024 features in FT-ICR spectra were found unique (Figure 1C). The observed unique *m/z* features are not unexpected if the differences in design of instruments, for example in terms of mass analyzers, ion path trajectories and ion detectors are considered.[11,27,28]

MS-type comparison – distinction of normal and tumor tissue samples

A formalin-fixed, paraffin-embedded (FFPE) tissue microarray (TMA) derived from normal and colon cancer tissue was taken as a model to examine the performance of FT-ICR and TOF obtained data for the classification of tissue types. Regions of interest were defined on

the H&E stained colon TMAs according to normal epithelium and tumor tissue followed by the generation of peak lists for the FT-ICR and TOF dataset. Principle component analyses (PCA) was applied on peak lists of each mass spectrometer to determine the level of segregation between spectra groups to separate tissue types on the basis of data distance and overlap (Figure 2). It was observed that spectra groups tended to separate along the first principal in the FT-ICR PCA (Figure 2A); however, overlapping data clouds occurred in the TOF PCA (Figure 2B). Statistical analysis found 42 significantly different *m/z* features in FT-ICR and 16 significantly different peaks in TOF distinguishing normal and tumor tissues samples (Table 1). Although more unique features with higher significance level could be achieved by FT-ICR MS all significant *m/z* features followed the same trend in both measurements demonstrating a similar data quality (Table 1). Ions which were detected very close to each other (less than 0.01 Da difference) were resolved by FT-ICR but not by TOF MSI. The importance of instrumental resolution in order to accurately separate the molecular masses is exemplified for the ion*s* *m/z* 241.003 and *m/z* 241.012 capable to significantly discriminate normal and tumor tissue samples by FT-ICR MS (Figure 3B, C). Both masses were detected with resolutions of R=73520 and R=72571, respectively. In contrast, the lower resolving power of TOF was not able to separate the closely associated ions leading to no statistically significant difference. Thus, TOF visualization diminished the molecular and statistical informative value (Figure 3D). A simulation of the TOF image can be achieved by combining the two signals (*m/z*=241.003 and 241.012) in the FT-ICR spectrum (Figure 3E). Small differences in the ion distribution maps might be due to variations in sensitivity between the mass spectrometers. One can speculate about the influence of ion stability of metabolites to in-source fragmentation affecting data differences between both instruments. It has been described that metastable decay of ions with labile groups like sulfates and phosphates (e.g. carbohydrates, glycoconjugates) can hinder the observation of the intact molecular ion in MALDI MS.[29-31] FT-ICR MS operate comparatively to TOF at a higher pressure with collisional cooling leading to softer ionization conditions.[30,32] Two adjacent ions at *m/z* 259.0135 and *m/z* 259.0226 detected by MALDI-FT-ICR MSI were examined in more detail. Both *m/z* species significantly distinguish normal epithelium and tumor colon tissue in MALDI-FT-ICR but not in MALDI-TOF MSI which combines both signals to *m/z* 259.025 (Table 1 and Figure S-3). The ion at *m/z* 256.0226 was identified by MALDI MS/MS analysis directly from the colon TMA as a hexose-6-phosphate. Moreover, the unambiguous peak for hexose-6-phosphate could be detected from fresh frozen and FFPE liver tissue demonstrating stability of this ion using both platforms (Figure S-3). Thus instrumental resolving power is putatively more affecting statistical differences than in source effects (see Table 1).

TOF visualizations of a tumor specific mass at *m/z* 181.966 with a resolution of R=3260 (in FTICR with R=95868) and a mucus specific mass at *m/z* 256.997 with R=3960 (FT-ICR with R=68641) presented comparable ion distribution maps of anatomical features in both datasets (Figure 4A). Further, representative tissue microarray cores display comparable visualizations such as *m/z* 256.997 localizing the mucus within colon tissue samples (Figure 4B). The MS-type comparison presents that MALDI-TOF in general could achieve identical results; however images and statistical analysis were associated with much more uncertainties. Overlaid peak information and background noise in TOF images made a precise assignment of molecular attributes characteristic for different tissue features (e.g. tumor, normal epithelium, etc.) more difficult and limited subsequent classification by PCA. Thus a global mapping of metabolites with regard to complex tissue samples benefitted from higher mass resolution as provided by FT-ICR MSI.

MS-type comparison – discovery of prognostic markers

Next, the capability of MALDI-TOF MSI was tested to reproduce the discovery of a prognostic marker which was previously identified by FT-ICR MSI in a TMA of esophageal adenocarcinoma patient samples: *m/z* 256.9975 was identified in univariate and multivariate analysis (with correction of cumulative alpha errors) to significantly correlate with disease-free survival independent of TMN classification (Figure 5A).[10] The chemical identity of *m/z* 256.9975 was assigned to deoxy sugar acid with ester sulfate present in mucus regions.[10] For the instrument comparison the next consecutive TMA section which underwent MSI by FT-ICR was measured by MALDI-TOF to maintain a high level of data consistency between the two measurements. Despite lower spectral resolution of MALDI-TOF MS a comparison of mean spectra obtained from both mass spectrometers revealed a high similarity (Figure 6). The magnification display enlarged the prognostic parameter which partially overlaps with neighboring peaks in the TOF spectrum at *m/z* 257.006 compared to the resolved FT-ICR peak at *m/z* 256.9975 (Figure 6). A comparison of peak intensities across patient sample cores showed a good correlation between both instrument types (Pearson's correlation coefficient=0.883) (Figure 7). Both peaks visualized the mucus regions in esophageal adenocarcinomas (Figure 5B, D). Although it was not possible to rediscover *m/z* 257.006 in the TOF data in an untargeted screening approach, a targeted univariate statistical analysis of TOF data found – in line with the prognostic value of *m/z* 256.9975 observed in the FT-ICR (Figure 5A) – also *m/z* 257.006 significantly correlated with patients' survival (Figure 5C). The reason for the failed untargeted screening approach might be a misclassification of four patients in the TOF data based on the mean compared to the FT-ICR data which is most likely caused by a loss of sensitivity and specificity (Figure 7). Summarized, our results

revealed that MALDI-TOF MS was not suitable to discover this particular prognostic marker which can subdivide patients into different prognostic groups. However, the advanced knowledge of the previous discovered prognostic marker based on mass spectral analyzes from high resolution MSI enabled to reproduce and verify results on the TOF imaging platform using univariate analysis.

CONCLUSION

Two different types of mass spectrometer, a MALDI-FT-ICR and a MALDI-TOF/TOF mass spectrometer were compared for comprehensive metabolite analysis with emphasis on clinical application of FFPE tissue samples. FT-ICR mass spectrometry benefitted from its inherently higher sensitivity and molecular specificity yielding more distinct ions with higher significance levels. These features supported separation of different tissue types using MALDI-FT-ICR MSI whereas MALDI-TOF MSI was not able to separate normal epithelium and tumor tissue in a classification approach using principle component analysis. Nevertheless, data analysis revealed some identical results between both mass spectrometers albeit statistical analyses were associated with higher uncertainties using the TOF instrument. A prognostic marker could be recovered with MALDI-TOF MSI, considering that targeted analysis was based on previous information received from FT-ICR MSI analysis. It can be concluded that a global mapping of metabolites from complex tissue samples is advantageous using high mass resolution imaging. Traditionally, promising biomarkers are validated (e.g. validation cohorts) for clinical use which is much more time consuming for the measurements and data analyzes because of a required increase of patient series.[33] When using FT-ICR MSI it is a challenge to keep data volume and acquisition time manageable whereas current developments in TOF instrumentation can avoid long measurement times. Thus, the advantages and drawbacks of both mass spectrometers give rise to use them combined in clinic-related metabolite analysis: high mass resolution devices should be preferred as discovery platform to identify prognostic markers whereas TOF and TOF/TOF MSI can alternatively be used to verify potential valuable biomarkers via targeted (e.g. SRM/MRM) analysis using validation cohorts.

ACKNOWLEDGMENTS

This project was funded by the Ministry of Education and Research of the Federal Republic of Germany (BMBF) (Grant No. 01ZX1310B, ERA-NET TRANSCAN-2-ARREST), and the Deutsche Forschungsgemeinschaft (Grant Nos/ HO 1254/3-1, SFB 824 TP Z02 and WA 1656/3-1) to AW. We thank Ulrike Buchholz, Claudia-Mareike Pflüger, and Gabriele

Mettenleiter for their excellent technical assistance.

REFERENCES

(1) Balluff, B.; Rauser, S.; Meding, S.; Elsner, M.; Schone, C.; Feuchtinger, A.; Schuhmacher, C.; Novotny, A.; Jutting, U.; Maccarrone, G.; Sarioglu, H.; Ueffing, M.; Braselmann, H.; Zitzelsberger, H.; Schmid, R. M.; Hofler, H.; Ebert, M. P.; Walch, A. Am. J. Pathol. 2011, 179, 2720-2729.
(2) Lazova, R.; Seeley, E. H.; Keenan, M.; Gueorguieva, R.; Caprioli, R. M. Am. J. Dermatopathol. 2012, 34, 82-90.
(3) Powers, T. W.; Holst, S.; Wuhrer, M.; Mehta, A. S.; Drake, R. R. Biomolecules 2015, 5, 2554-2572.
(4) Prideaux, B.; Via, L. E.; Zimmerman, M. D.; Eum, S.; Sarathy, J.; O'Brien, P.; Chen, C.; Kaya, F.; Weiner, D. M.; Chen, P. Y.; Song, T.; Lee, M.; Shim, T. S.; Cho, J. S.; Kim, W.; Cho, S. N.; Olivier, K. N.; Barry, C. E., 3rd; Dartois, V. Nat. Med. 2015, 21, 1223-1227.
(5) Jones, E. E.; Powers, T. W.; Neely, B. A.; Cazares, L. H.; Troyer, D. A.; Parker, A. S.; Drake, R. R. Proteomics 2014, 14, 924-935.
(6) Kelly, A. D.; Breitkopf, S. B.; Yuan, M.; Goldsmith, J.; Spentzos, D.; Asara, J. M. PLoS One 2011, 6, e25357.
(7) Yuan, M.; Breitkopf, S. B.; Yang, X.; Asara, J. M. Nat. Protoc. 2012, 7, 872-881.
(8) Wojakowska, A.; Marczak, L.; Jelonek, K.; Polanski, K.; Widlak, P.; Pietrowska, M. PLoS One 2015, 10, e0136902.
(9) Wojakowska, A.; Chekan, M.; Marczak, L.; Polanski, K.; Lange, D.; Pietrowska, M.; Widlak, P. Mol. Cell Endocrinol. 2015.
(10) Buck, A.; Ly, A.; Balluff, B.; Sun, N.; Gorzolka, K.; Feuchtinger, A.; Janssen, K. P.; Kuppen, P. J.; van de Velde, C. J.; Weirich, G.; Erlmeier, F.; Langer, R.; Aubele, M.; Zitzelsberger, H.; Aichler, M.; Walch, A. J. Pathol. 2015, 237, 123-132.
(11) Scigelova, M.; Hornshaw, M.; Giannakopulos, A.; Makarov, A. Mol. Cell Proteomics 2011, 10, M111 009431.
(12) Marshall, A. G.; Guan, S. H. Rapid Commun. Mass Spectrom. 1996, 10, 1819-1823.
(13) Marshall, A. G.; Blakney, G. T.; Chen, T.; Kaiser, N. K.; McKenna, A. M.; Rodgers, R. P.; Ruddy, B. M.; Xian, F. Mass. Spectrom. (Tokyo) 2013, 2, S0009.
(14) Hopfgartner, G. Bioanalysis 2011, 3, 121-123.
(15) Pelander, A.; Decker, P.; Baessmann, C.; Ojanpera, I. J. Am. Soc. Mass Spectrom. 2011, 22, 379-385.
(16) Ogrinc Potocnik, N.; Porta, T.; Becker, M.; Heeren, R. M.; Ellis, S. R. Rapid Commun. Mass Spectrom. 2015, 29, 2195-2203.
(17) Spraggins, J. M.; Caprioli, R. M. J. Am. Soc. Mass Spectrom. 2011, 22, 1022-1031.
(18) Trim, P. J.; Djidja, M. C.; Atkinson, S. J.; Oakes, K.; Cole, L. M.; Anderson, D. M.; Hart, P. J.; Francese, S.; Clench, M. R. Anal. Bioanal. Chem. 2010, 397, 3409-3419.
(19) Buck, A.; Halbritter, S.; Spath, C.; Feuchtinger, A.; Aichler, M.; Zitzelsberger, H.; Janssen, K. P.; Walch, A. Anal. Bioanal. Chem. 2015, 407, 2107-2116.
(20) Huber, K.; Aichler, M.; Sun, N.; Buck, A.; Li, Z.; Fernandez, I. E.; Hauck, S. M.; Zitzelsberger, H.; Eickelberg, O.; Janssen, K. P.; Keller, U.; Walch, A. Histochem. Cell Biol. 2014, 142, 361-371.
(21) Ye, H.; Wang, J.; Greer, T.; Strupat, K.; Li, L. ACS Chem. Neurosci. 2013, 4, 1049-1056.
(22) Kind, T.; Fiehn, O. BMC Bioinformatics 2007, 8, 105.
(23) Kumari, S.; Stevens, D.; Kind, T.; Denkert, C.; Fiehn, O. Anal. Chem. 2011, 83, 5895-5902.
(24) Erve, J. C.; Gu, M.; Wang, Y.; DeMaio, W.; Talaat, R. E. J. Am. Soc. Mass Spectrom. 2009, 20, 2058-2069.
(25) Strohalm, M.; Kavan, D.; Novak, P.; Volny, M.; Havlicek, V. Anal. Chem. 2010, 82, 4648-4651.

(26) Pietrowska, M.; Gawin, M.; Polanska, J.; Widlak, P. Proteomics 2016.
(27) Suckau, D.; Resemann, A.; Schuerenberg, M.; Hufnagel, P.; Franzen, J.; Holle, A. Anal. Bioanal. Chem. 2003, 376, 952-965.
(28) Trim, P. J.; Snel, M. F. Methods 2016.
(29) Zhang, J.; Lamotte, L.; Dodds, E. D.; Lebrilla, C. B. Anal. Chem. 2005, 77, 4429-4438.
(30) O'Connor, P. B.; Costello, C. E. Rapid. Commun. Mass Spectrom. 2001, 15, 1862-1868.
(31) Soltwisch, J.; Souady, J.; Berkenkamp, S.; Dreisewerd, K. Anal. Chem. 2009, 81, 2921-2934.
(32) Ivleva, V. B.; Elkin, Y. N.; Budnik, B. A.; Moyer, S. C.; O'Connor, P. B.; Costello, C. E. Anal. Chem. 2004, 76, 6484-6491.
(33) Feng, Z.; Prentice, R.; Srivastava, S. Pharmacogenomics 2004, 5, 709-719.

FIGURE LEGENDS

Table 1. Comparison of statistically significant ions (Wilcoxon rank-sum test) discriminating tumor and normal colon epithelium. Arrows indicate high or low signal intensity values in tumor regions compared to normal epithelium. (n.s. - not significant).

Figure 1. (A) Peak picking with different signal-to-noise ratios from mass spectra derived from MALDI-FT-ICR and MALDI-TOF MS. **(B)** Number of FT-ICR ions detected within the Full Width at Half Maximum (FWHM) window of TOF MS peaks. **(C)** Bar plots showing common and unique ions from both instruments sorted according to the mass range.

Figure 2. Principel compononent analysis (PCA) score plot applied to the spectra groups from normal epithelium (green) and tumor (red). **(A)** PCA from MALDI-FT-ICR data distinguished normal epithelium from tumor tissue whereas **(B)** PCA from MALDI-TOF data was not able to separate the different tissue types.

Figure 3. (A) H&E stained colon TMA with annotated regions of normal epithelium (green) and tumor (red). Mass spectra and ion distribution maps showing differences in significance levels and localization of the ions **(B)** *m/z* 241.003 ± 0.005 (green) and **(C)** *m/z* 241.012 ± 0.005 (red) with MALDI-FT-ICR and MALDI-TOF MSI. **(D)** In high mass resolution imaging the two analytes are clearly defined as different molecular components discriminating normal colon epithelium and tumor in MALDI-FT-ICR MSI. Imaging with lower resolution combined signals making it appear as a single peak. In the TOF image a superimposition of green and red results in yellow demonstrating ion co-localization. **(E)** Simulation of the TOF image by the selection of a wider bin width (mass range used for image generation) combined both peaks (*m/z* 241.007 ± 0.010) in FT-ICR spectrum. This example also ilustrates the necessity of high mass resolution to distinguish tissue types in classification approaches using global spectral peaks. (n.s. - not significant).

Figure 4. Resolved peaks obtained from MALDI-FT-ICR and MALDI-TOF reveal ion images of the same anatomical features. **(A)** Selection of the ions *m/z* 181.966 and *m/z* 256.997 localize tumor (red) and mucus (green), respectively. **(B)** Images of representative tissue microarray cores display the localization of *m/z* 181.966 and *m/z* 256.997 overlaid on corresponding H&E-stained samples from MALDI-FT-ICR and MALDI-TOF MSI.

Figure 5. MS-type comparison for addressing the finding of a prognostic marker of patient survival outcome (n=53). **(A)** Uni- and multivariate statistical analyses of MALDI-FT-ICR data correlated *m/z* 256.9975 significantly with disease-free survival (p=0.00154), independently of other survival determinants given by the clinical TNM classification (inset; p=0.034). **(C)** MALDI-TOF analysis showed that the signal *m/z* 257.006 can significantly distinguish patients outcome (p=0.0101). However, this finding was not significant after multivariate analysis (inset; p=0.260). **(B)** and **(D)** showing ion distribution maps of the corresponding signals in mucus regions of esophageal adenocarcinomas (blue). Panels **(A)** and **(B)** adapted from Buck, A.; Ly, A.; Balluff, B.; Sun, N.; Gorzolka, K.; Feuchtinger, A.; Janssen, K. P.; Kuppen, P. J.; van de Velde, C. J.; Weirich, G.; Erlmeier, F.; Langer, R.; Aubele, M.; Zitzelsberger, H.; Aichler, M.; Walch, High-resolution MALDI-FT-ICR MS imaging for the analysis of metabolites from formalin-fixed, paraffin-embedded clinical tissue samples, J. Pathol., Vol. 237, Issue 1 (ref 10). Copyright © 2015 Pathological Society of Great Britain and Ireland. Published by John Wiley & Sons, Ltd.

Figure 6. Comparison between the average mean spectra recorded by MALDI-FT-ICR and MALDI-TOF mass spectrometry. The insets show enlarged the same prognostic parameter at **(A)** *m/z* 256.9975 and **(B)** *m/z* 257.006 which significantly correlated with patients disease-free survival.

Figure 7. Comparison of peak intensities across patient sample cores between *m/z* 256.9975 (MALDI-FT-ICR, abscissa) and *m/z* 257.006 (MALDI-TOF, ordinate). The correlation between both instrument types was calculated by Pearson's correlation (coefficient=0.883). As for the prognostic analysis (see Figure 5), patients were divided into two groups based on the 50% peak intensity threshold (red lines). Based on that classification rule, four patients were classified differently between MALDI-FT-ICR and MALDI-TOF, as obeserved in quadrants Q1 and Q4.

Table 1.

	MALDI-FT-ICR MS (7T solariX)		MALDI-TOF MS (Ultraflex III)	
m/z [M-H]$^-$	p-Value	SR	p-Value	SR
152.002	0.000148	↑	0.008934	↑
152.996	0.001285	↑	0.078799	
167.997	0.000798	↑	0.162953	
171.007	0.001625	↑	0.085530	
181.966	0.000148	↑	0.028624	↑
183.963	0.000148	↑	0.028624	↑
192.889	0.022867	↑	0.433247	
209.961	0.000148	↑	0.031193	↑
216.871	0.003354	↑	0.278951	
217.930	0.001380	↑	0.033913	↑
219.927	0.007337	↑	0.003466	↑
234.882	0.008122	↑	0.138645	
241.003	0.002395	↓	0.263682	
241.012	0.002105	↑	0.263682	
242.015	0.001824	↑	0.008934	↑
251.967	0.000873	↑	0.635337	
256.997	0.002395	↓	0.009435	↓
259.014	0.000732	↓	0.538581	
259.023	0.000873	↑	0.538581	
282.029	0.001263	↑	0.028624	↑
298.024	0.001011	↑	0.854723	
300.040	0.000790	↑	0.077131	
315.031	0.002404	↑	0.746113	
315.053	0.000798	↑	0.746113	
324.044	0.001908	↑	0.635337	
333.059	0.000873	↑	0.206383	
382.090	0.002395	↓	0.009435	↓
384.088	0.002395	↓	0.073281	
386.108	0.011675	↓	0.538581	
396.058	0.001285	↑	0.127149	
401.983	0.001380	↑	0.877941	
412.055	0.001011	↑	0.076230	
424.101	0.00973	↓	0.028624	↓
425.105	0.020915	↓	0.433247	
426.086	0.005022	↓	0.102898	
428.086	0.023272	↓	0.098573	
437.269	0.001380	↑	0.389175	
444.082	0.002395	↓	0.015441	↓
590.138	0.005022	↓	0.028624	↓
599.320	0.000790	↑	0.022475	↑
600.322	0.000990	↑	0.026649	↑
606.134	0.013963	↓	0.013928	↓

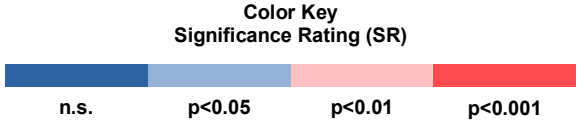

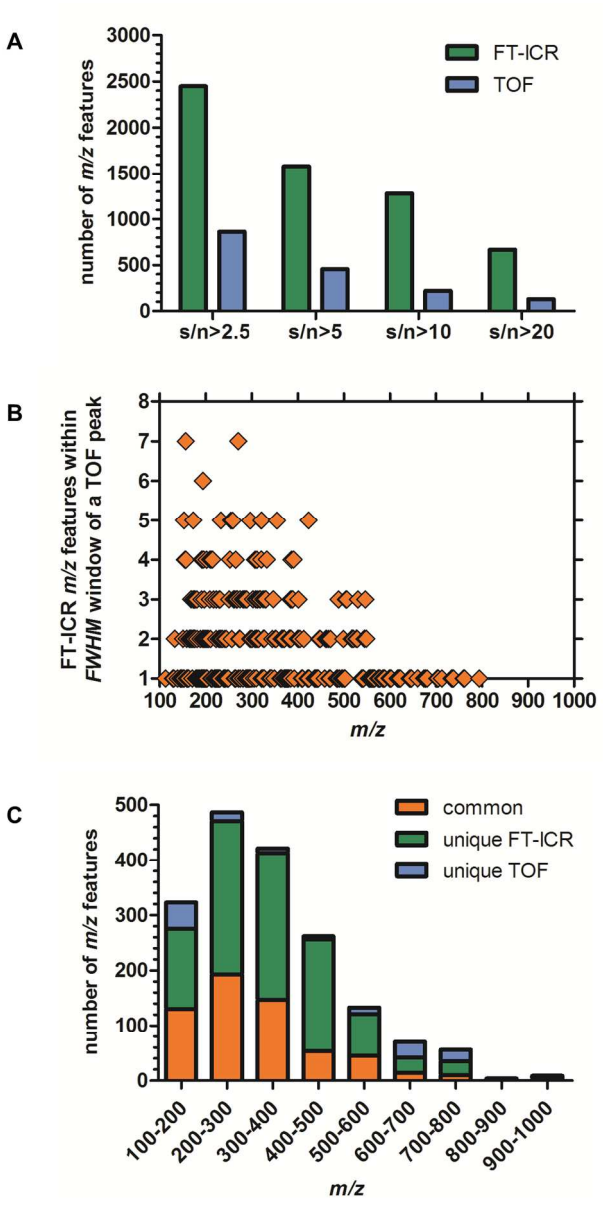

Figure 1: (A) Peak picking with different signal-to-noise ratios from mass spectra derived from MALDI-FT-ICR and MALDI-TOF MS. (B) Number of FT-ICR ions detected within the Full Width at Half Maximum (FWHM) window of TOF MS peaks. (C) Bar plots showing common and unique ions from both instruments sorted according to the mass range.
106x208mm (300 x 300 DPI)

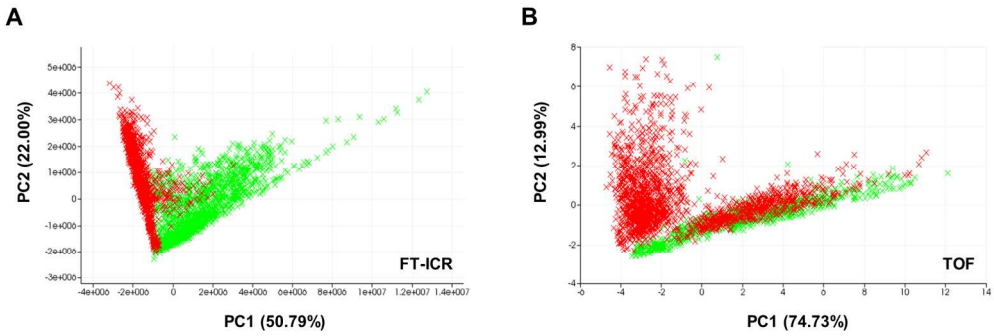

Figure 2: Principel compononent analysis (PCA) score plot applied to the spectra groups from normal epithelium (green) and tumor (red). (A) PCA from MALDI-FT-ICR data distinguished normal epithelium from tumor tissue whereas (B) PCA from MALDI-TOF data was not able to separate the different tissue types.
166x56mm (300 x 300 DPI)

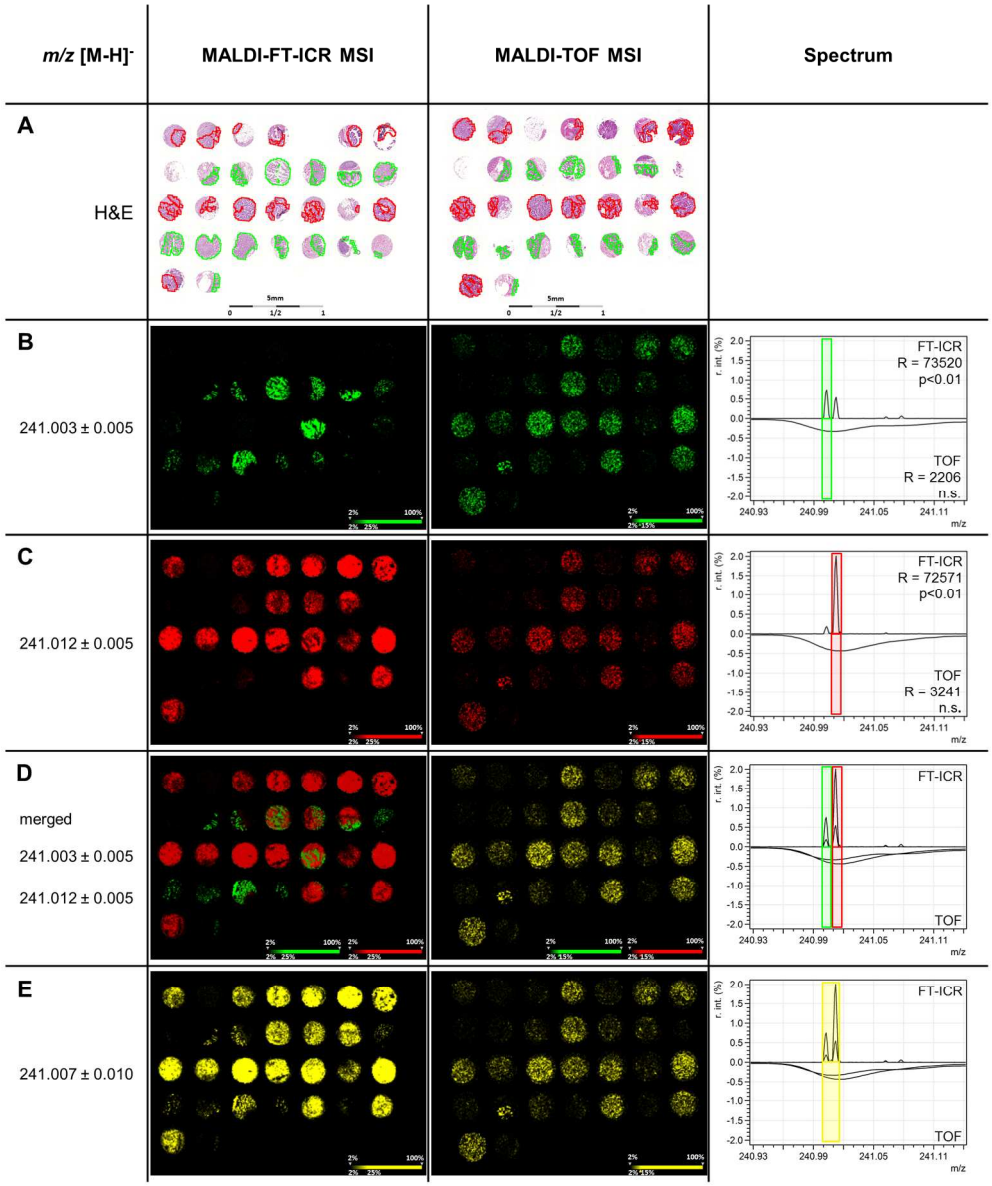

Figure 3: (A) H&E stained colon TMA with annotated regions of normal epithelium (green) and tumor (red). Mass spectra and ion distribution maps showing differences in significance levels and localization of the ions (B) m/z 241.003 ± 0.005 (green) and (C) m/z 241.012 ± 0.005 (red) with MALDI-FT-ICR and MALDI-TOF MSI. (D) In high mass resolution imaging the two analytes are clearly defined as different molecular components discriminating normal colon epithelium and tumor in MALDI-FT-ICR MSI. Imaging with lower resolution combined signals making it appear as a single peak. In the TOF image a superimposition of green and red results in yellow demonstrating ion co-localization. (E) Simulation of the TOF image by the selection of a wider bin width (mass range used for image generation) combined both peaks (m/z 241.007 ± 0.010) in FT-ICR spectrum. This example also illustrates the necessity of high mass resolution to distinguish tissue types in classification approaches using global spectral peaks.
171x204mm (300 x 300 DPI)

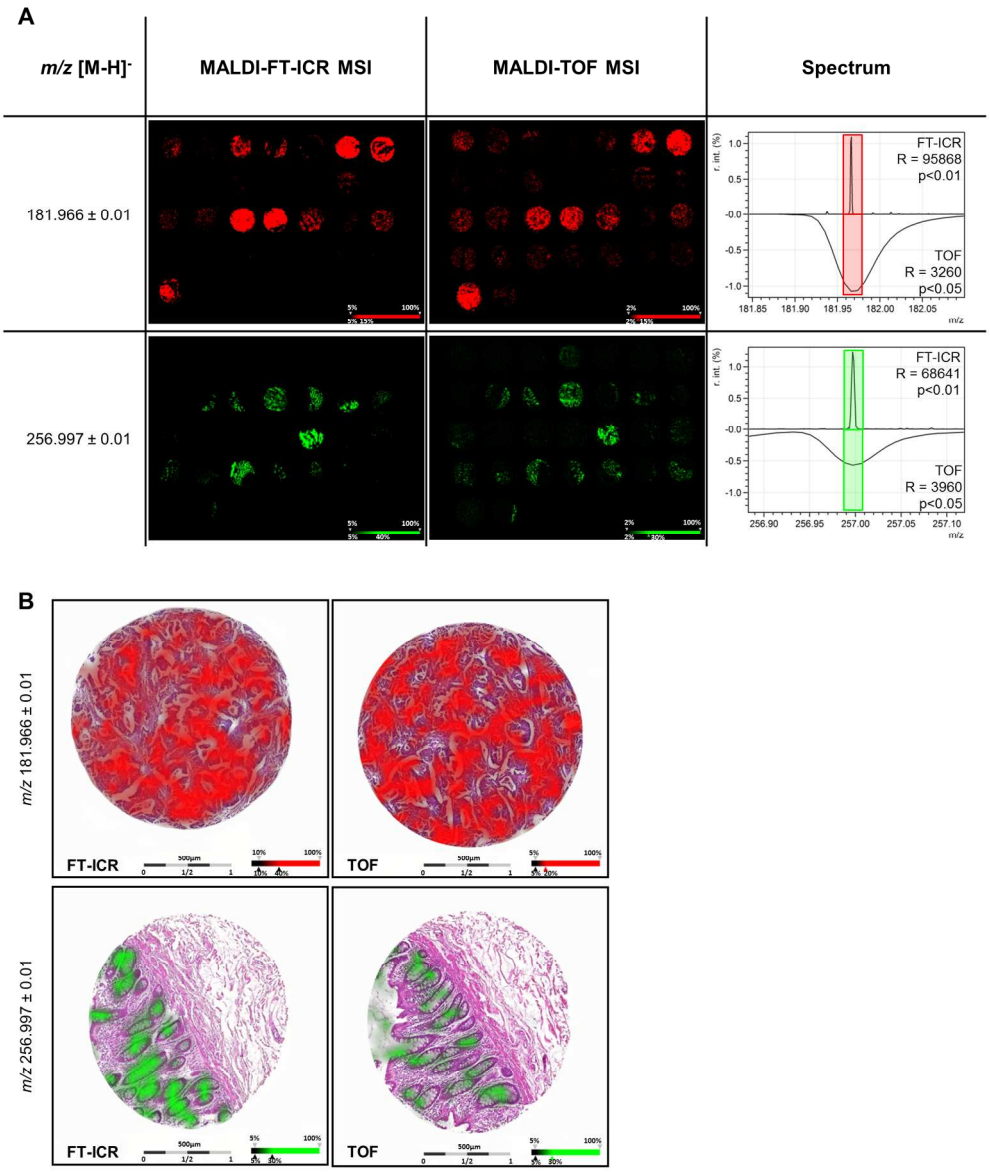

Figure 4: Resolved peaks obtained from MALDI-FT-ICR and MALDI-TOF reveal ion images of the same anatomical features. (A) Selection of the ions m/z 181.966 and m/z 256.997 localize tumor (red) and mucus (green), respectively. (B) Images of representative tissue microarray cores display the localization of m/z 181.966 and m/z 256.997 overlaid on corresponding H&E-stained samples from MALDI-FT-ICR and MALDI-TOF MSI.
171x202mm (300 x 300 DPI)

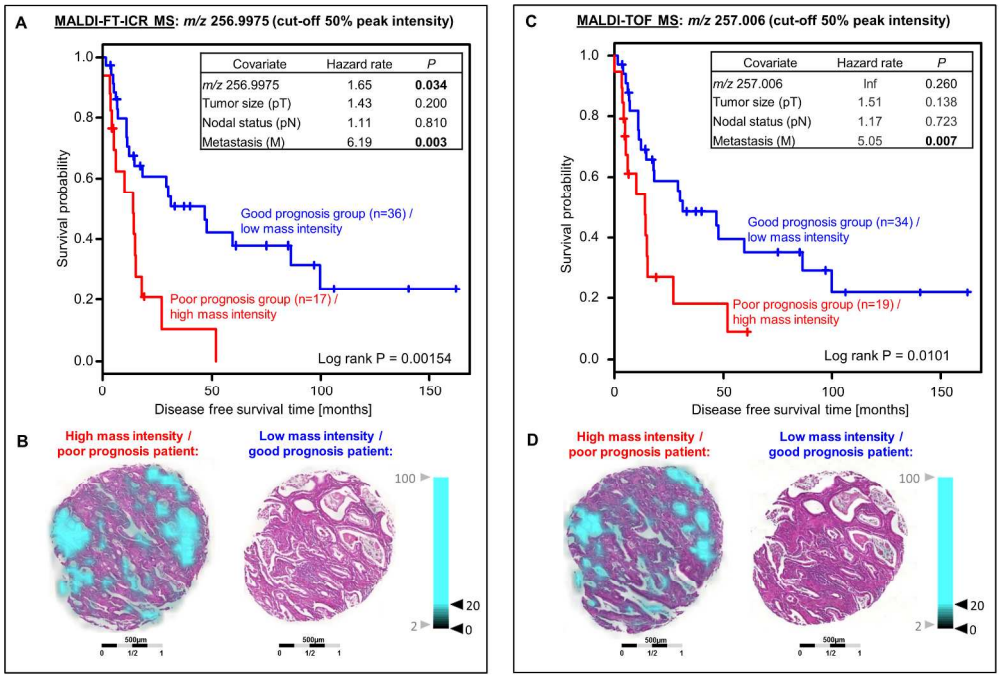

Figure 5: MS-type comparison for addressing the finding of a prognostic marker of patient survival outcome (n=53). (A) Uni- and multivariate statistical analyses of MALDI-FT-ICR data correlated m/z 256.9975 significantly with disease-free survival (p=0.00154), independently of other survival determinants given by the clinical TNM classification (inset; p=0.034). This figure is adapted with permission from reference 10. (C) MALDI-TOF analysis showed that the signal m/z 257.006 can significantly distinguish patients outcome (p=0.0101). However, this finding was not significant afer multivariate analysis (inset; p=0.260). (B) and (D) showing ion distribution maps of the corresponding signals in mucus regions of esophageal adenocarcinomas (blue).
238x161mm (300 x 300 DPI)

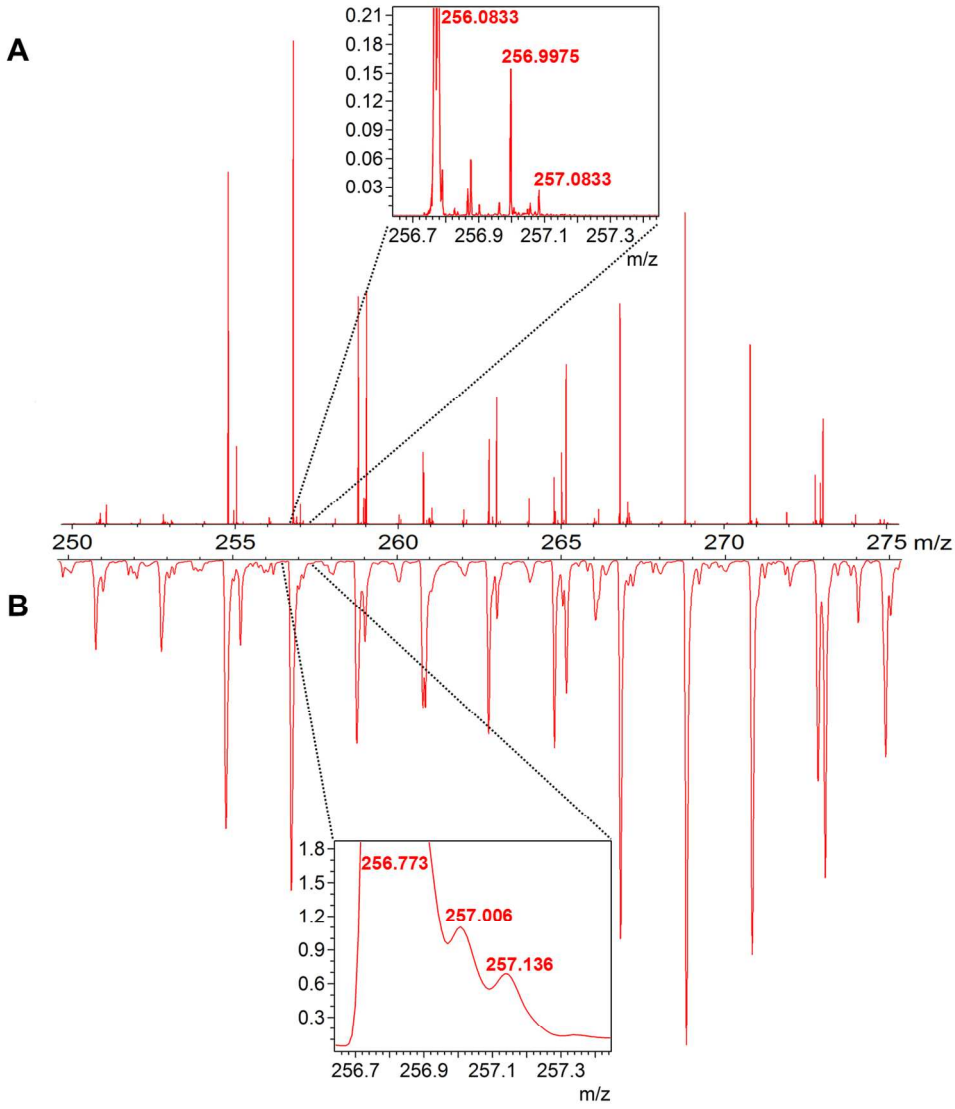

Figure 6: Comparison between the average mean spectra recorded by MALDI-FT-ICR and MALDI-TOF mass spectrometry. The insets show enlarged the same prognostic parameter at (A) m/z 256.9975 and (B) m/z 257.006 which significantly correlated with patients disease-free survival.
129x148mm (300 x 300 DPI)

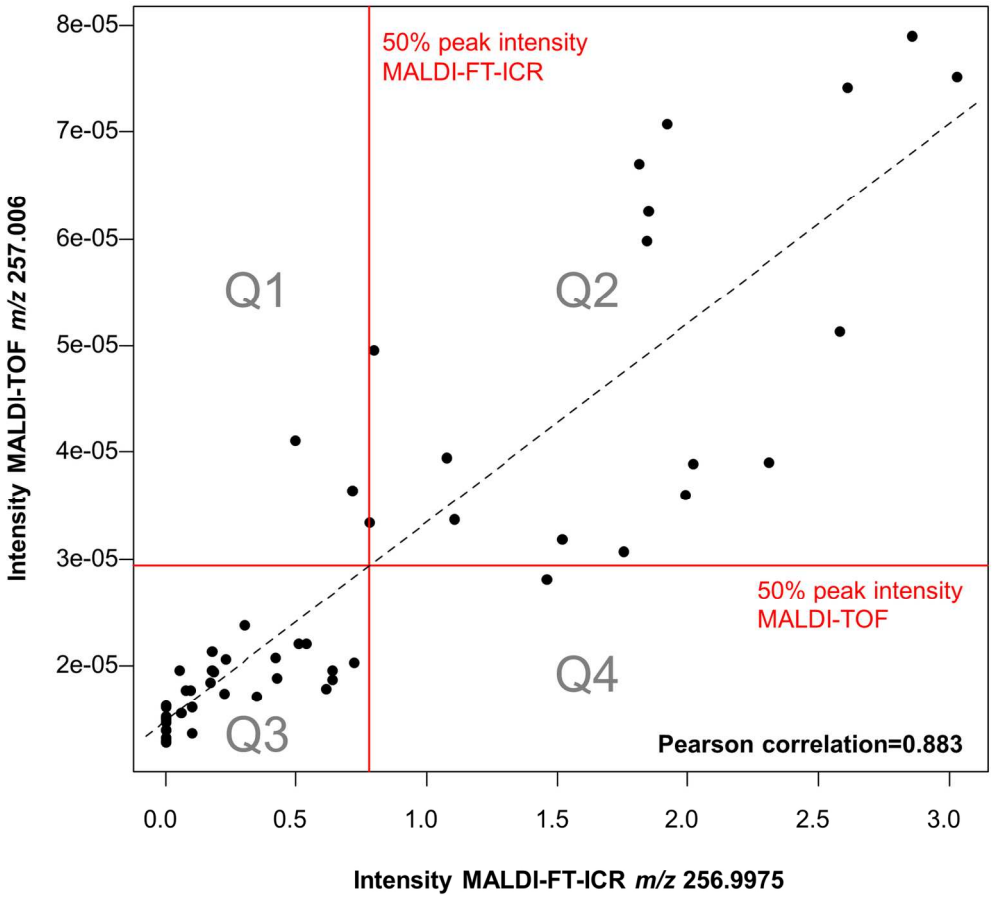

Figure 7: Comparison of peak intensities across patient sample cores between m/z 256.9975 (MALDI-FT-ICR, abscissa) and m/z 257.006 (MALDI-TOF, ordinate). The correlation between both instrument types was calculated by Pearson's correlation (coefficient=0.883). As for the prognostic analysis (see Figure 5), patients were divided into two groups based on the 50% peak intensity threshold (red lines). Based on that classification rule, four patients were classified differently between MALDI-FT-ICR and MALDI-TOF, as obeserved in quadrants Q1 and Q4.
155x140mm (300 x 300 DPI)

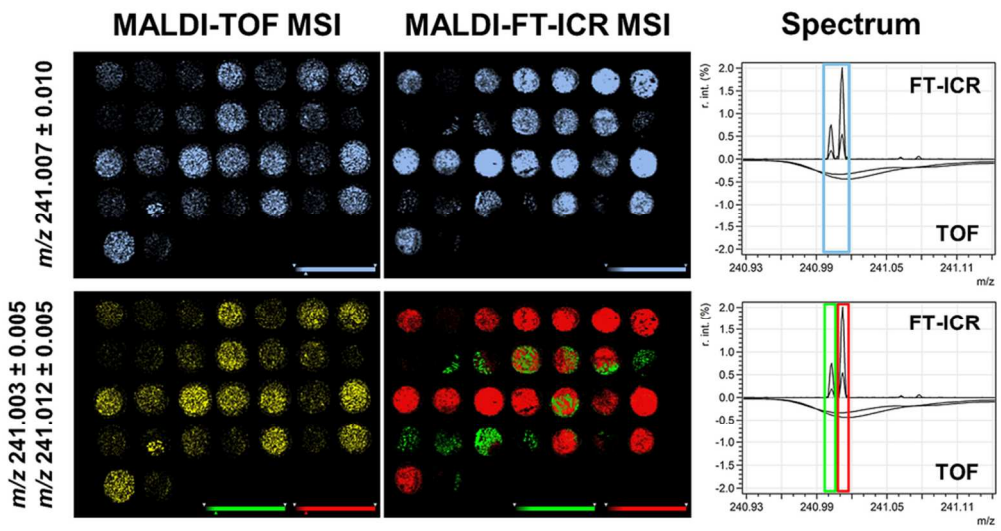

For TOC Only
86x45mm (300 x 300 DPI)